2020 IEEE/RSJ International Conference on Intelligent Robots and Systems (IROS)
October 25-29, 2020, Las Vegas, NV, USA (Virtual)

Identification of a Human Hand Kinematics by Measuring and Merging of Nail-Based Finger Motions

Hidenori Tani[1], Ryo Nozawa[1] and Tomomichi Sugihara[2,3]

***Abstract*— A method to identify the kinematics model of a human hand that less suffers from the skin artifact is proposed based on a fact that the movements of nails with respect to the corresponding fingertip bones are much smaller than that of skin. It consists of two stages. In the first (individual) stage, the most likely combination of joint assignments and angles of each finger is identified through a dual-phase least squares method (LSM), where the joint angles are estimated in the inner LSM and the joint assignments in the outer LSM, from the movement of the hand dorsum with respect to the base coordinate frame attached to each nail. In the second (merging) stage, kinematic models of each finger are merged so as to compromise the estimated movements of the hand dorsum by them also through the dual-phase LSM. It is shown that the identified joint assignments have an advantage over several existing anthropomorphic robot hands based on the distribution of pinchability (DOP), which is also proposed in this paper as a novel index to evaluate the ability of in-hand manipulation.**

I. Introduction

Versatile robot hands that can manipulate objects dexterously have been demanded in order to automate complex tasks that only humans can do under the current technology. It is a reasonable idea to design such robot hands in similar forms to human hands since the anthropomorphism is exploited for intuitive implementations and teaching of humans' skills for task executions. Although it is not trivial how to quantify the humans' manipulation skills, the authors think that a good starting point for it is to model a hand that captures kinematic characteristics of the human hand.

Some anatomical works identified joint axes of human fingers through cadaveric measurement [1], [2], [3]. While they found that humans' finger joints can be approximated by combining revolute joints to some extent, they also showed that the centers of rotations of the joints vary during motions due to sliding and rolling of bones. It means that the kinematic characteristics of the human hand cannot be fully reconstructed by simply connecting locally identified joint structures. Hence, dynamic movements of fingertips, which cannot be measured by the above *in vitro* approaches, should be taken into account for an accurate modeling of the human hand particularly from the viewpoint of task executions.

This work was supported by Grant-in-Aid for Scientific Research (B) #18H03310, Ministry of Education, Culture, Sports, Science and Technology-Japan.

[1]Hidenori Tani and Ryo Nozawa are with Kawasaki Heavy Industry. This work was done when they used to be students of Osaka University, Japan.

[2]Tomomichi Sugihara is with Graduate School of Engineering, Osaka University, 2–1 Yamadaoka, Suita, Osaka, Japan.

[3]Tomomichi Sugihara is with Preferred Networks, Inc., 1–6–1 Otemachi, Chiyoda-ku, Tokyo, Japan. zhidao@ieee.org

Several works to identify joint assignments of a human hand through *in vivo* measurement with MRI [4], [5], [6] and optical motion capture systems [7], [8] have also been made. Whichever devices are used, a difficulty in measuring the hand in motion is how to supress an effect of the skin artifact; it is hard to find a rigid part in a human hand with which the coordinate frame to describe movements of the markers can be associated since the human hand is covered by soft skin, which frequently shrinks and expands during motions. Some approaches by applying Kalman filter in order to reduce the effect as a noise [9] and by explicitly estimating drifts of each marker due to deformation of skin [6] were taken in order to solve this issue.

This paper proposes another method than the above to identify the kinematics model of a human hand more easily. A key fact is that the movements of a nail with respect to the distal phalanx is negligibly small in general. Based on this, the proposed method consists of two stages. In the first stage, the most likely combination of joint assignments and angles of each finger is identified through a dual-phase least squares method (LSM), where the joint angles are estimated by the inner LSM and the joint assignments by the outer LSM, from the movement of the hand dorsum with respect to the base coordinate frame attached to the nail. An ill-posedness of the joint assignments is resolved by referring nominal centers of joints designated by markers. In the second stage, the kinematic models of each finger are merged so as to compromise the estimated movements of the hand dorsum by them also through the dual-phase LSM. Another contribution of this paper is to show that the identified kinematics model has an advantage over several existing anthropomorphic robot hands based on *the distribution of pinchability* (DOP), which is also proposed in this paper as a novel index to evaluate the ability of in-hand manipulation.

II. Kinematics model of a human hand and marker arrangement

Fig. 1 shows the kinematics model of a human hand employed in this work. It is branched from a fixed point in the palm to five fingers and the forearm. Though such a fixed root point is fictitious, it represents movements of the carpal bones and is supposed to be on the hand dorsum for an approximation. Note that the objective of this work is not to reconstruct an anatomically detailed mechanism but to find a reasonable joint assignments for mechanical design. The movements of fingers are modeled by combinations of revolute joints. Each finger except for the thumb has 1-DOF distal interphalangeal (DIP) joint, 1-DOF proximal

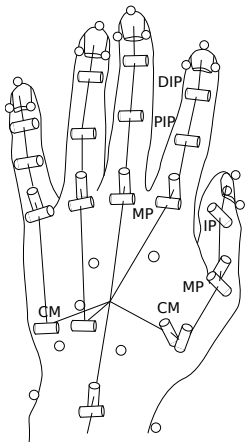

Fig. 1. Kinematics model of a human hand consisting of 25 revolute joints

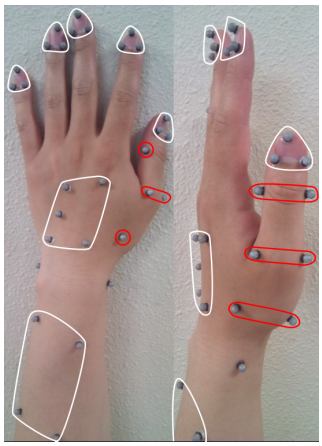

Fig. 2. An example of marker arrangements (white: primary markers, red:auxiliary markers)

interphalangeal (PIP) joint and 2-DOF metacarpophalangeal (MP) joint. The thumb has 1-DOF interphalangeal (IP) joint, 2-DOF MP joint and 2-DOF carpometacarpal (CM) joint. In addition, the ring and pinky fingers have 1-DOF CM joints, which are coaxial with each other but move independently. Two revolute joints at the wrist are optional. Hence, the model has 25 DOFs in total.

As detailed in the next section, the identification process is two-staged. In the first *individual stage*, motions of markers attached on each finger are measured by a motion capture system and the kinematics model of the finger is identified from them. Then, motions of the markers on the whole hand are measured, based on which the individual finger models are merged at the hand dorsum in the second *merging stage*. Let us call the measurement experiments in each stage *the individual sessions* and *the merging session*, respectively. Fig. 2 shows an example arrangement of markers for the measurement sessions. The markers grouped by white loops (*primary markers*) are used in all the sessions, while that grouped by red loops (*auxiliary markers*) are only in the individual sessions. The primary markers include 3×5 markers on the nail, 5 on the hand dorsum, 4 on the forearm and 2 on the wrist, respectively. The auxiliary markers are attached to both ends of "guessed" joint axes of the finger of interest (the thumb in the case of the figure) as pairs. They do not provide reliable estimation of the joint assignments but help to resolve the ill-posedness in the identification in addition to define the initial guess.

III. Two-staged identification process of nail-based finger kinematics

A. Problem set-up and outline

Let us assign numbers from 1 to 5 to the thumb, index, middle, ring and pinky fingers, respectively, and count the number of joints of the ith finger ($i = 1, \cdots, 5$) by n_i, i.e., $\{n_i\} = \{5, 4, 4, 5, 5\}$. The nail frame $\Sigma_{\mathrm{N}i}$ and joint frames Σ_{ij} ($j = 1, \cdots, n_i$) are assigned on the ith finger such that z-axis of Σ_{ij} is aligned with the jth joint axis. The hand dorsum frame Σ_{D} and the forearm frame Σ_{W} are also attached. Any Σ_* of the above is defined by a combination of

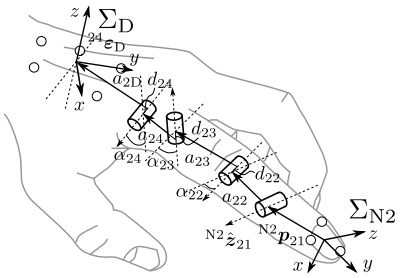

Fig. 3. Parameters to define joint assignments (example: index finger)

position of the origin $\boldsymbol{p}_*$ and a 3×3 attitude matrix $\boldsymbol{R}_*$. The joint assignment of each finger is described by a kinematic chain defined by the following constant parameters.

${}^{\mathrm{N}i}\boldsymbol{p}_{i1}$: position of the origin of Σ_{i1} with respect to $\Sigma_{\mathrm{N}i}$

${}^{\mathrm{N}i}\hat{\boldsymbol{z}}_{i1}$: direction of the z-axis of Σ_{i1} with respect to $\Sigma_{\mathrm{N}i}$

$(a_{ij}, s_{ij}, c_{ij}, d_{ij})$: relative assignment of the jth joint with respect to the $j-1$th joint, where $s_{ij} \stackrel{\mathrm{def}}{=} \sin\alpha_{ij}$, $c_{ij} \stackrel{\mathrm{def}}{=} \cos\alpha_{ij}$, and $(a_{ij}, \alpha_{ij}, d_{ij}, q_{ij})$ with the jth joint angle q_{ij} conforms to a modified DH notation [10]

$a_{\mathrm{D}i}$: distance between the origins of Σ_{in_i} and Σ_{D}

${}^{in_i}\boldsymbol{\epsilon}_{\mathrm{D}}$: Euler parameters (a unit quaternion) that represents the attitude of Σ_{D} with respect to Σ_{in_i}

${}^{\mathrm{N}i}\hat{\boldsymbol{z}}_{i1}$, s_{ij}, c_{ij} and ${}^{in_i}\boldsymbol{\epsilon}_{\mathrm{D}}$ have to satisfy

$$\|{}^{\mathrm{N}i}\hat{\boldsymbol{z}}_{i1}\| = 1, \quad s_{ij}^2 + c_{ij}^2 = 1, \quad \|{}^{in_i}\boldsymbol{\epsilon}_{\mathrm{D}}\| = 1. \tag{1}$$

Fig. 3 illustrates those parameters of the index finger. Let

$$\boldsymbol{\phi}_{\mathrm{N}i} \stackrel{\mathrm{def}}{=} ({}^{\mathrm{N}i}\boldsymbol{p}_{i1}, {}^{\mathrm{N}i}\hat{\boldsymbol{z}}_{i1}) \tag{2}$$

$$\boldsymbol{\phi}_{\mathrm{J}i} \stackrel{\mathrm{def}}{=} \{(s_{ij}, c_{ij}, a_{ij}, d_{ij})\} \quad (j = 1, \cdots, n_i - 1) \tag{3}$$

$$\boldsymbol{\phi}_{\mathrm{D}i} \stackrel{\mathrm{def}}{=} (a_{\mathrm{D}i}, {}^{in_i}\boldsymbol{\epsilon}_{\mathrm{D}}) \tag{4}$$

$$\boldsymbol{\phi}_i \stackrel{\mathrm{def}}{=} (\boldsymbol{\phi}_{\mathrm{N}i}, \boldsymbol{\phi}_{\mathrm{J}i}, \boldsymbol{\phi}_{\mathrm{D}i}) \tag{5}$$

$$\boldsymbol{\phi} \stackrel{\mathrm{def}}{=} \{\boldsymbol{\phi}_i\} \quad (i = 1, \cdots, 5) \tag{6}$$

$$\boldsymbol{q}_i \stackrel{\mathrm{def}}{=} \{q_{ij}\} \quad (j = 1, \cdots, n_i) \tag{7}$$

$$\boldsymbol{q} \stackrel{\mathrm{def}}{=} \{\boldsymbol{q}_i\} \quad (i = 1, \cdots, 5). \tag{8}$$

The size of $\boldsymbol{\phi}$ is 122 since $a_{\mathrm{D}4} = a_{\mathrm{D}5}$ and ${}^{4n_4}\boldsymbol{\epsilon}_{\mathrm{D}} = {}^{5n_5}\boldsymbol{\epsilon}_{\mathrm{D}}$ due to the coaxial arrangement, while that of $\boldsymbol{q}$ is 23, where the optional wrist joints are omitted from $\boldsymbol{q}$. $\boldsymbol{\phi}$ and $\boldsymbol{q}$ uniquely determines the configuration of the hand.

Let us denote $\mathcal{M}_* = \{\boldsymbol{p}_{\mathrm{M}*j}\}$ ($j = 1, \cdots, n_{\mathrm{M}*}$) a set of positions of the primary markers, where $* = \mathrm{D}$ is for the hand dorsum with $n_{\mathrm{MD}} = 5$, and $* = \mathrm{N}i$ for the nail of the ith finger with $n_{\mathrm{MN}i} = 3$. A series of $\mathcal{M}[k] = \{\mathcal{M}_*\}[k]$ at discrete time $k = 0, \cdots, N-1$, where N (~ 1000 in an ordinary session) is the number of sampled frames, is measured according to a protocol described in the next section, and the corresponding series of $\{\Sigma_*\}[k]$ is computed from them as follows. $\Sigma_*[0]$ are defined such that $\boldsymbol{p}_*[0]$ is the barycenter of $\mathcal{M}_*[0]$, the direction of z-axis $\hat{\boldsymbol{z}}_*[0]$ is the unit eigenvector corresponding to the minimum eigenvalue of the covariance matrix of $\mathcal{M}_*[0]$, and the direction of x-axis $\hat{\boldsymbol{x}}_*[0]$ is the normalized $\boldsymbol{p}_{\mathrm{M}*1}[0] - \boldsymbol{p}_*[0]$. The ensuing $\Sigma_*[k]$ ($k = 1, \cdots, N-1$) are computed based on Horn et al.'s method

[11]. Then, a series of the relative formations of $\Sigma_{\mathrm{D}}[k]$ with respect to $\Sigma_{\mathrm{N}i}[k]$, $\Sigma_{\mathrm{N}i\to\mathrm{D}}[k] = ({}^{\mathrm{N}i}\boldsymbol{p}_{\mathrm{D}}[k], {}^{\mathrm{N}i}\boldsymbol{R}_{\mathrm{D}}[k])$ $(i = 1, \cdots, 5)$, are obtained. The objective here is to find the most likely combination of the joint assignments $\boldsymbol{\phi}$ and a series of joint angles $\boldsymbol{q}[k]$ of the hand that reproduces the series of $\{\Sigma_{\mathrm{N}i\to\mathrm{D}}\}[k]$. Note that $\boldsymbol{q}[k]$ varies depending on k, whereas $\boldsymbol{\phi}$ is constant in all the sessions, and hence, the number of parameters to be estimated is $23N + 122$. This work takes an approach to find so many parameters by solving two-staged dual-phase least squares problem rather than a batch optimization. A combination of $\boldsymbol{\phi}_i$ and $\boldsymbol{q}_i[k]$ is individually identified in the individual stage, and then, $\boldsymbol{\phi}_i$ $(i = 1, \cdots, 5)$ are merged into the most likely $\boldsymbol{\phi}$ in the merging stage. In each stage, $\boldsymbol{q}_i[k]$/$\boldsymbol{q}[k]$ with respect to the up-to-date $\boldsymbol{\phi}_i$/$\boldsymbol{\phi}$ is found in the inner LSM, while $\boldsymbol{\phi}_i$/$\boldsymbol{\phi}$ is updated through the outer LSM. The actual computation processes are detailed in the following subsections.

B. Individual stage

$\boldsymbol{q}_i[k]$ is found from $({}^{\mathrm{N}i}\boldsymbol{p}_{\mathrm{D}}[k], {}^{\mathrm{N}i}\boldsymbol{R}_{\mathrm{D}}[k])$ and $\mathcal{M}[k]$ provided $\boldsymbol{\phi}_i$ by solving the inverse kinematics. It is basically unsolvable since $n_i < 6$ for $\forall i$, and thus, formulated as a least squares problem with an error function defined as

$$E_{\mathrm{IK}i}[k] \stackrel{\mathrm{def}}{=} E_{\mathrm{D}i}[k] + w_{\mathrm{J}} \sum_{j=1}^{n_i} E_{\mathrm{J}ij}[k], \tag{9}$$

where

$$E_{\mathrm{D}i}[k] \stackrel{\mathrm{def}}{=} \boldsymbol{e}_{\mathrm{P}i}^{\mathrm{T}}[k]\boldsymbol{W}_{\mathrm{P}}\boldsymbol{e}_{\mathrm{P}i}[k] + \boldsymbol{e}_{\mathrm{A}i}^{\mathrm{T}}[k]\boldsymbol{W}_{\mathrm{A}}\boldsymbol{e}_{\mathrm{A}i}[k] \tag{10}$$

$$\boldsymbol{e}_{\mathrm{P}i}[k] \stackrel{\mathrm{def}}{=} {}^{\mathrm{N}i}\boldsymbol{p}_{\mathrm{D}}[k] - {}^{\mathrm{N}i}\tilde{\boldsymbol{p}}_{\mathrm{D}}[k] \tag{11}$$

$$\boldsymbol{e}_{\mathrm{A}i}[k] \stackrel{\mathrm{def}}{=} \boldsymbol{a}\left({}^{\mathrm{N}i}\boldsymbol{R}_{\mathrm{D}}[k]\,{}^{\mathrm{N}i}\tilde{\boldsymbol{R}}_{\mathrm{D}}^{\mathrm{T}}[k]\right), \tag{12}$$

${}^{\mathrm{N}i}\tilde{\boldsymbol{p}}_{\mathrm{D}}[k]$ and ${}^{\mathrm{N}i}\tilde{\boldsymbol{R}}_{\mathrm{D}}[k]$ are the reproduced ${}^{\mathrm{N}i}\boldsymbol{p}_{\mathrm{D}}[k]$ and ${}^{\mathrm{N}i}\boldsymbol{R}_{\mathrm{D}}[k]$ from given $\boldsymbol{q}_i[k]$ and $\boldsymbol{\phi}_i$, respectively, $\boldsymbol{a}(\boldsymbol{R})$ for ${}^{\forall}\boldsymbol{R} \in \mathrm{SO}(3)$ is the equivalent angle-axis vector with $\boldsymbol{R}$ [12], $\boldsymbol{W}_{\mathrm{P}}$ and $\boldsymbol{W}_{\mathrm{A}}$ are weighting matrices, $E_{\mathrm{J}ij}[k]$ is an additional evaluation function explained later, and w_{J} is its weight.

$E_{\mathrm{J}ij}[k]$ in Eq. (9) works for regularizing the problem. Even though the number of joints of each finger is less than 6, the inverse kinematics still has a redundancy issue in which DIP joints might flip. It is also known [13] that the identification of nearly parallel consecutive axes is sensitive to the numerical error. In order to resolve the instability of computation due to the above, "guessed" joint axes are given by the auxiliary markers attached on the subject's hand (refer Fig. 2 again). For 1-DOF joints, reasonable guesses are suggested by the paired markers and the sum of distances from the two markers to the modeled axis is evaluated, while for 2-DOF joints, the guesses are not reliable and the sum of distances from the midpoint of the paired markers to the modeled two axes is added. Fig. 4 depicts the idea. $\boldsymbol{q}_i[k]$ is estimated by solving the following least squares problem:

$$\boldsymbol{q}_i[k] = \arg\min_{\boldsymbol{q}_i} E_{\mathrm{IK}i}(\boldsymbol{q}_i; \boldsymbol{\phi}_i, \mathcal{M}[k]). \tag{13}$$

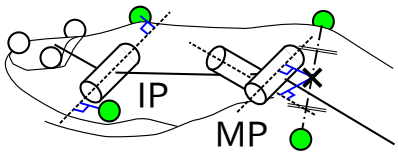

Fig. 4. Guessed joint axes from auxiliary markers for regularization

The above solution gives the minimized error $E^*_{\mathrm{IK}i}[k] = E_{\mathrm{IK}i}(\boldsymbol{q}_i[k]; \boldsymbol{\phi}_i, \mathcal{M}[k])$. The total error E_i is defined as

$$E_i \stackrel{\mathrm{def}}{=} \sum_{k=0}^{N-1} E^*_{\mathrm{IK}i}[k]. \tag{14}$$

The most likely $\boldsymbol{\phi}_i$ is obtained by minimizing E_i. During the computation, ${}^{\mathrm{N}i}\hat{\boldsymbol{z}}_{i1}$, (s_{ij}, c_{ij}) and ${}^{in_i}\boldsymbol{\epsilon}_{\mathrm{D}}$ are normalized everytime in order to satisfy Eq. (1). An optional technique to improve accuracy is to decrease $\boldsymbol{w}_{\mathrm{J}}$ gradually with iteration.

C. Merging stage

The skin artifact particularly reduces reliability of $\boldsymbol{\phi}_{\mathrm{D}i}$ $(i = 1, \cdots, 5)$ more than $\boldsymbol{\phi}_{\mathrm{N}i}$ and $\boldsymbol{\phi}_{\mathrm{J}i}$. They are corrected also through the dual-phase LSM in the merging stage. Let us define $\tilde{\Sigma}_{\mathrm{D}i}[k]$ by cascading $\Sigma_{\mathrm{N}i}[k]$ with $\Sigma_{\mathrm{N}i\to\mathrm{D}}[k]$ reproduced from $\boldsymbol{q}_i[k]$ and $\boldsymbol{\phi}_i$, namely,

$$\tilde{\boldsymbol{p}}_{\mathrm{D}i}[k] = \boldsymbol{p}_{\mathrm{N}i}[k] + \boldsymbol{R}_{\mathrm{N}i}[k]\,{}^{\mathrm{N}i}\tilde{\boldsymbol{p}}_{\mathrm{D}}[k] \tag{15}$$

$$\tilde{\boldsymbol{R}}_{\mathrm{D}i}[k] = \boldsymbol{R}_{\mathrm{N}i}[k]\,{}^{\mathrm{N}i}\tilde{\boldsymbol{R}}_{\mathrm{D}}[k]. \tag{16}$$

Though $\Sigma_{\mathrm{D}}[k]$ is uniquely determined from $\mathcal{M}_{\mathrm{D}}[k]$, $\tilde{\Sigma}_{\mathrm{D}i}[k]$ $(i = 1, \cdots, 5)$ are different from each other due to the error of identification. The objective of the inner LSM in this stage is to find $\boldsymbol{q}[k]$ that compromises those differences as

$$\boldsymbol{q}[k] = \arg\min_{\boldsymbol{q}} \left(\sum_{i=1}^{5} E_{\mathrm{IK}i}[k] + \sum_{(i,j)\in\mathcal{I}_{\mathrm{M}}} E_{\mathrm{D}ij}[k] \right), \tag{17}$$

where

$$E_{\mathrm{D}ij}[k] \stackrel{\mathrm{def}}{=} \boldsymbol{e}_{\mathrm{P}ij}^{\mathrm{T}}[k]\boldsymbol{W}_{\mathrm{P}}\boldsymbol{e}_{\mathrm{P}ij}[k] + \boldsymbol{e}_{\mathrm{A}ij}^{\mathrm{T}}[k]\boldsymbol{W}_{\mathrm{A}}\boldsymbol{e}_{\mathrm{A}ij}[k] \tag{18}$$

$$\mathcal{I}_{\mathrm{M}} \stackrel{\mathrm{def}}{=} \{(1,2),(2,3),(3,4),(4,5),(5,1)\} \tag{19}$$

$$\boldsymbol{e}_{\mathrm{P}ij}[k] \stackrel{\mathrm{def}}{=} \tilde{\boldsymbol{p}}_{\mathrm{D}i}[k] - \tilde{\boldsymbol{p}}_{\mathrm{D}j}[k] \tag{20}$$

$$\boldsymbol{e}_{\mathrm{A}ij}[k] \stackrel{\mathrm{def}}{=} \boldsymbol{a}\left(\tilde{\boldsymbol{R}}_{\mathrm{D}i}[k]\tilde{\boldsymbol{R}}_{\mathrm{D}j}^{\mathrm{T}}[k]\right). \tag{21}$$

This is also the inverse kinematics problem.

The most likely position $\tilde{\boldsymbol{p}}_{\mathrm{D}}[k]$ and attitude $\tilde{\boldsymbol{R}}_{\mathrm{D}}[k]$ of $\Sigma_{\mathrm{D}}[k]$ are obtained by avaraging $\tilde{\boldsymbol{p}}_{\mathrm{D}i}[k]$ and $\tilde{\boldsymbol{R}}_{\mathrm{D}i}[k]$, respectively. Their covariance matrices are also computed as

$$\boldsymbol{S}_{\mathrm{DP}}[k] = \sum_{i=1}^{5} \boldsymbol{W}_{\mathrm{P}}\tilde{\boldsymbol{e}}_{\mathrm{P}i}[k]\tilde{\boldsymbol{e}}_{\mathrm{P}i}^{\mathrm{T}}[k]\boldsymbol{W}_{\mathrm{P}}^{\mathrm{T}} \tag{22}$$

$$\boldsymbol{S}_{\mathrm{DA}}[k] = \sum_{i=1}^{5} \boldsymbol{W}_{\mathrm{A}}\tilde{\boldsymbol{e}}_{\mathrm{A}i}[k]\tilde{\boldsymbol{e}}_{\mathrm{A}i}^{\mathrm{T}}[k]\boldsymbol{W}_{\mathrm{A}}^{\mathrm{T}}, \tag{23}$$

where

$$\tilde{\boldsymbol{e}}_{\mathrm{P}i}[k] \stackrel{\mathrm{def}}{=} \tilde{\boldsymbol{p}}_{\mathrm{D}}[k] - \tilde{\boldsymbol{p}}_{\mathrm{D}i}[k] \tag{24}$$

$$\tilde{\boldsymbol{e}}_{\mathrm{A}i}[k] \stackrel{\mathrm{def}}{=} \boldsymbol{a}\left(\tilde{\boldsymbol{R}}_{\mathrm{D}}[k]\tilde{\boldsymbol{R}}_{\mathrm{D}i}^{\mathrm{T}}[k]\right). \tag{25}$$

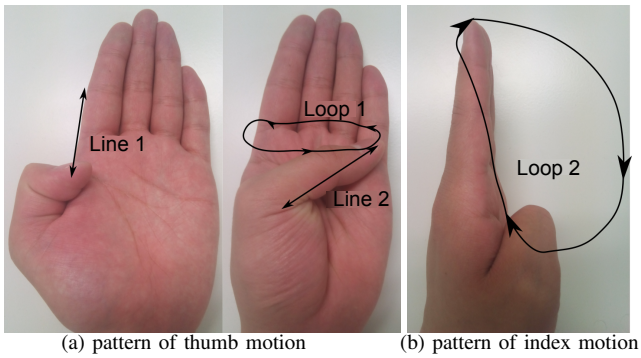

(a) pattern of thumb motion (b) pattern of index motion

Fig. 5. Patterns for excitations of joint motions

Finally, the most likely $\{\boldsymbol{\phi}_{\mathrm{D}i}\}$ $(i = 1, \cdots, 5)$ is obtained by minimizing the above variance through the outer LSM as

$$\{\boldsymbol{\phi}_{\mathrm{D}i}\} = \arg\min_{\{\boldsymbol{\phi}_{\mathrm{D}i}\}} \sum_{k=0}^{N-1} (E^{*}_{\mathrm{IK}i}[k] + w_{\mathrm{SP}} \|\boldsymbol{S}_{\mathrm{DP}}[k]\| + w_{\mathrm{SA}} \|\boldsymbol{S}_{\mathrm{DA}}[k]\|), \quad (26)$$

where w_{SP} and w_{SA} are weights.

IV. Identification of Kinematics Model

A. Protocol of measurement sessions

This section describes a protocol to excite motions of joints to be identified in the measurement sessions. Fig. 5 (a) shows spatial trajectories that the tip of the thumb tracks in the individual session. The motion along Line 1 excites the flexion-extention movements of IP and MP joints in particular, whereas the effect of the skin artifact around CMC joint is suppressed by maximally abducting the finger. The motion along Line 2 highlights the abduction-adduction motion of CMC joint. The motion along Loop 1 sweeps the boundary of the thumb's workspace.

In each individual session for the other four fingers, flexsion-extention movement of PIP joint is measured first, and a coupled movement of PIP and DIP joints second. After that, Loop 2 drawn in Fig. 5 (b) is tracked by the fingertip in order to excite the flexion-extention movement of MP joint and sweep the boundary of the finger's workspace. The abduction-adduction movement of MP joint is also measured independently. In the sessions of the ring and pinky fingers, a movement of CM joint is additionally measured.

In the merging session, the excitation movements of each finger as well as the individual session and motions to touch the palm by each fingertip are newly observed one-by-one.

VENUS3D system (Nobby Tech. Ltd.) with 11 infrared cameras (sampling rate=100 Hz) was used for measurement.

B. Result and evaluation of accuracy

The proposed method was implemented with Sugihara method [12] for the inner LSM and Nelder-Mead method [14] for the outer LSM. The motion measurement sessions were conducted on a 23-year-old healthy male subject, and the kinematics model of the subject's left hand was identified. The weighting matrices were set for $\boldsymbol{W}_{\mathrm{P}} = \mathrm{diag}\{1/0.005^2, 1/0.005^2, 1/0.002^2\}$ and $\boldsymbol{W}_{\mathrm{A}} = \mathrm{diag}\{1/0.19^2, 1/0.19^2, 1/0.09^2\}$, respectively, which suppresses translational/twisting variances in/about normal direction to the hand surface, based on the range of deviation of the attached markers. For the other parameters, $w_{\mathrm{SP}} = w_{\mathrm{SP}} = 1$, and w_{J} was heuristically set for 1, $1/5$, $1/10$, $1/20$, $1/40$ and $1/60$ at each iteration, respectively.

TABLE I

Identified DH parameters (unit:mm for a and d, rad for α and θ)

	Thumb	Index	Middle	Ring	Pinky
	Base-CM1	Base-MP1	Base-MP1	Base-CM	Base-CM
α	1.64	1.64	1.64	1.64	1.64
θ	-1.49	-0.21	-0.48	-0.79	-1.07
a	2.93	2.93	2.93	2.93	2.93
d	-210.16	-17.53	-11.76	-67.49	-71.13
α	2.73	1.33	1.38	1.72	1.75
θ	-1.22	2.75	2.35	-1.83	-1.00
a	53.63	32.95	29.64	63.07	42.42
d	-213.94	13.59	-24.52	-60.22	-83.65
	CM1-CM2	MP1-MP2	MP1-MP2	CM-MP1	CM-MP1
α	1.56	-1.45	-2.14	0.09	0.27
a	-1.72	2.51	-1.17	55.60	56.92
d	13.79	-22.32	8.36	4.60	7.94
	CM2-MP1	MP2-PIP	MP2-PIP	MP1-MP2	MP1-MP2
α	-0.91	-1.71	0.91	1.50	1.20
a	17.2	34.25	45.15	3.05	0.96
d	26.4	-3.73	-6.36	8.67	17.15
	MP1-MP2	PIP-DIP	PIP-DIP	MP2-PIP	MP2-PIP
α	2.11	0.10	-0.06	1.75	1.58
a	-0.39	19.9	25.65	41.21	24.61
d	-10.84	-3.04	-2.33	0.33	5.95
	MP2-IP			PIP-DIP	PIP-DIP
α	-1.38			0.07	0.36
a	26.05			25.29	17.49
d	-6.22			-1.53	-6.72

TABLE II

Deviation of the hand dorsum frames associated with each finger from the identified frame

finger ID	Position		Attitude	
	standard deviation [mm]	maximum deviation [mm]	standard deviation [rad]	maximum deviation [rad]
1	0.36	1.16	0.018	0.059
2	0.58	2.14	0.028	0.111
3	0.48	1.86	0.021	0.074
4	0.47	1.79	0.025	0.073
5	0.57	2.48	0.027	0.126
	1.34	3.19	0.053	0.140

The identified joint assignments equivalently converted to DH parameters of a branched kinematic chain from the hand dorsum frame to the nail frames are shown in Table I. Note that the transformation from the first movable joint of each finger to the hand dorsum frame is represented by two sets of fixed DH parameters, and θs in the other sets are variable joint angles. An image of the model is visualized in Fig. 6.

Table II shows standard/maximum deviations of error between $\tilde{\Sigma}_{\mathrm{D}i}$ $(i = 1, \cdots, 5)$ and their average frame $\bar{\Sigma}_{\mathrm{D}}$, and also between Σ_{D} and $\bar{\Sigma}_{\mathrm{D}}$ on the bottom row. All the values of the former are less than the latter. It should be additionally noted that $3 \sim 5$ mm deviations of markers on the hand dorsum due to the deformation of the skin were observed. Comparing to it, the hand dorsum frame reproduced from the model corrected in the merging phase are less variant than that directly determined from $\mathcal{M}_{\mathrm{D}}[k]$, which means that the proposed nail-based method presents a more likely kinematics model than a naive hand-dorsum-based method.

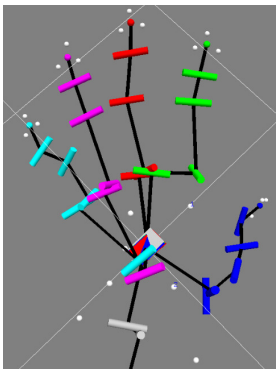

Fig. 6. Identified hand kinematics

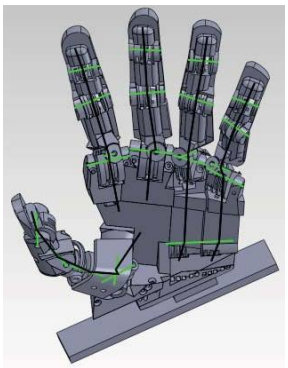

Fig. 7. A mechanical hand design

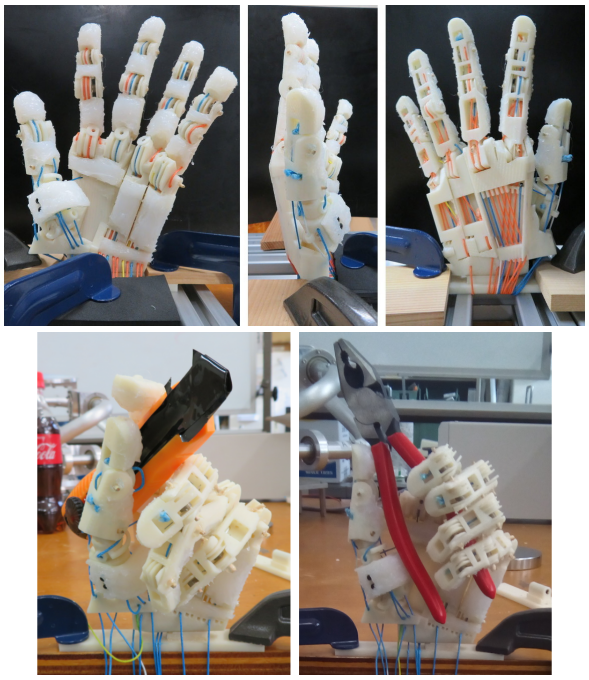

Fig. 8. 3D-printed prototype of the mechanism

C. Evaluation based on DOP

Figs. 7 and 8 show a robot hand mechanism designed based on the identified model and its 3D-printed prototype, respectively. An observation tells that it has a characteristic structure in which the flexion-extention joint axes are helically arranged as if it wraps the in-hand space from DIP to MP rather than aligned in parallel to each other. This seems that human fingers have a natural mechanism to get together in hand, which encourages cooperative multifingered motion. *The distribution of pinchability* (DOP) has been devised in this work to quantify the above characteristics from the viewpoint of the ability to oppose the thumb. Pinchability is measured by the number of fingertips that can reach a point, and DOP is defined as a volume of in-hand space where tips of the thumb and other fingers can reach.

The workspace of each fingertip of the identified hand model is depicted in Fig. 9 together with some other anthropomorphic robot hands (Gifu hand III [15], Shadow hand [16], Dexmart hand [17], and Elumotion hand 2 [18]), the kinematic dimensions of which have been publicized, for comparison. Since the volume of workspace depends on the size of the hand, they were normalized in a longitudinal direction by the sum of the lengths of fingers and in a lateral direction by the gap between the index and middle fingers. The workspaces are visualized in a quantized way by colorizing grids that each fingertip can reach. It seems that individual workspaces of the fingertips of the identified hand model are not particularly large comparing with the others; in fact, that of the thumb is the smallest of the five. Then, let us see DOP, which is the intersection of them. Fig. 10 shows multiplicities of the individual workspaces at each grid by color. Obviously, the identified hand model has by far the highest DOP, namely, more grids with higher multiplicity than the other hands, in the in-hand space.

V. Conclusions

A method to identify a kinematics model of a human hand was proposed. It consists of two-staged dual-phase LSM to find most likely combinations of the joint angles and the joint assignments with respect to loci of markers measured by a motion capture system. A protocol to excite motions of joints to be identified was also devised. A kinematics model of a human hand was identified through the proposed method.

An idea to evaluate the hand kinematics based on DOP was proposed as an index of how multifingered in-hand manipulation is encouraged. The identified hand model was evaluated with DOP and found to have even higher score than some acknowledged anthropomorphic robot hands.

References

[1] A. Hollister, "The Axes of Rotation of the Thumb Carpometacarpal Joint," *Journal of Orthopaedic Research*, vol. 10, pp. 454–460, 1992.

[2] A. Hollister, D. J. Giurintano, W. L. Buford, L. M. Myers, and A. Novick, "The axes of rotation of the thumb interphalangeal and metacarpophalangeal joints," *Clinical orthopaedics and related research*, no. 320, pp. 188–193, 1995.

[3] V. J. Santos and F. J. Valero-Cuevas, "Anatomical variability naturally leads to multimodal of Denavit-Hartenberg parameters for the human thumb," in *Proceedings of the 25th IEEE Annual International Conference of the Engineering in Medicine and Biology Society*, 2003, pp. 1823–1826.

[4] N. Miyata, M. Kouch, M. Mochimaru, and T. Kurihara, "Finger Joint Kinematics from MR Images," in *Proceedings of the 2005 IEEE/RSJ International Conference on Intelligent Robots and Systems*, 2005, pp. 2750–2755.

[5] G. Stillfried, U. Hillenbrand, M. Settles, and P. van der Smagt, "MRI-based skeletal hand movement model," *The human hand as an inspiration for robot hand development*, pp. 49–75, 2014.

[6] M. Gabiccini, G. Stillfried, H. Marino, and M. Bianchi, "A data-driven kinematic model of the human hand with soft-tissue artifact compensation mechanism for grasp synergy analysis," in *Proceedings of the 2013 IEEE/RSJ International Conference on Intelligent Robots and Systems*, 2013, pp. 3738–3745.

[7] P. Cerveri, E. D. Momi, N. Lopomo, G. Baud-Bovy, R. M. L. Barros, and G. Ferrigno, "Finger Kinematic Modeling and Real-Time Hand Motion Estimation," *Annals of Biomedical Engineering*, vol. 35, no. 11, pp. 1989–2002, 2007.

[8] L. Y. Chang and N. S. Pollard, "Method for Determining Kinematic Parameters of the In Vivo Thumb Carpometacarpal Joint," *IEEE Transactions on Biomedical Engineering*, vol. 55, no. 7, pp. 1897–1906, 2008.

[9] P. Cerveri, A. Pedotti, and G. Ferrigno, "Kinematical models to reduce the effect of skin artifacts on marker-based human motion estimation," *Journal of Biomechanics*, vol. 38, pp. 2228–2236, 2005.

[10] W. Khalil and E. Dombre, *Modeling, identification and control of robots*. Taylor Francis, 2002.

[11] B. K. P. Horn, "Closed-form solution of absolute orientation using unit quaternions," *Journal of the Optical Society of America*, vol. 4, no. 4, pp. 629–642, 1987.

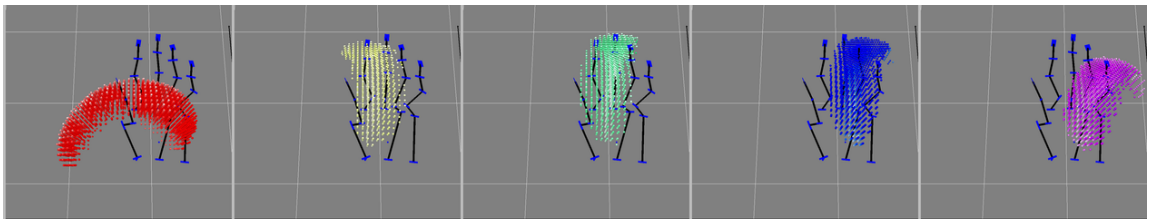

(a) the identified hand model

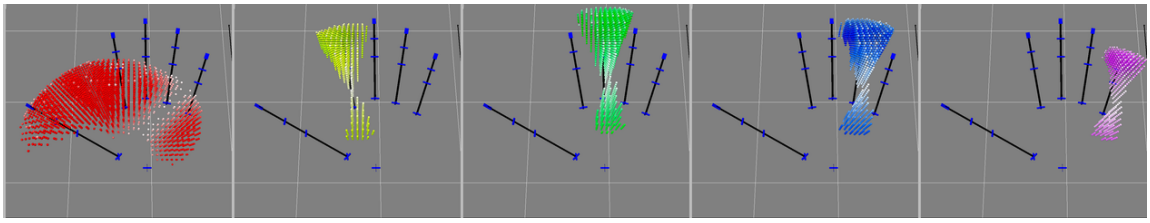

(b) Gifu hand III [15]

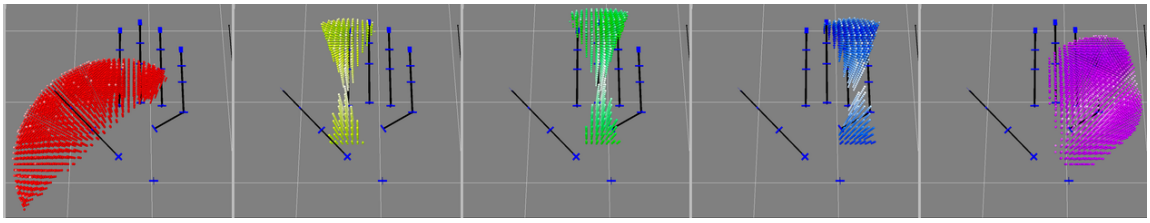

(c) Shadow hand [16]

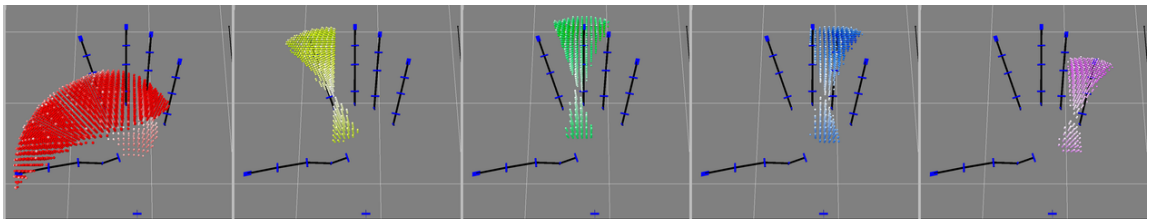

(d) Dexmart hand [17]

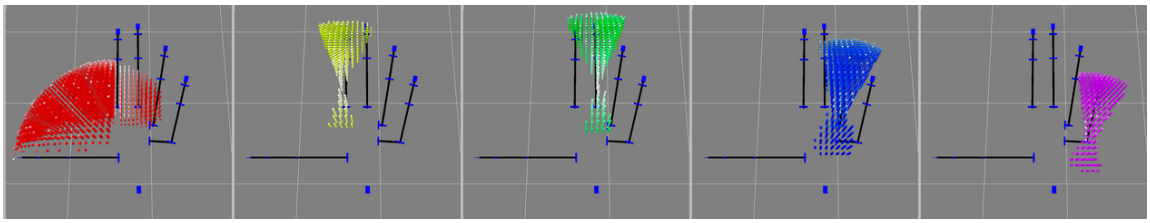

(e) Elumotion Hand 2 [18]

Fig. 9. Workspace of each finger of the identified hand model compared with some other anthropomorphic robot hands

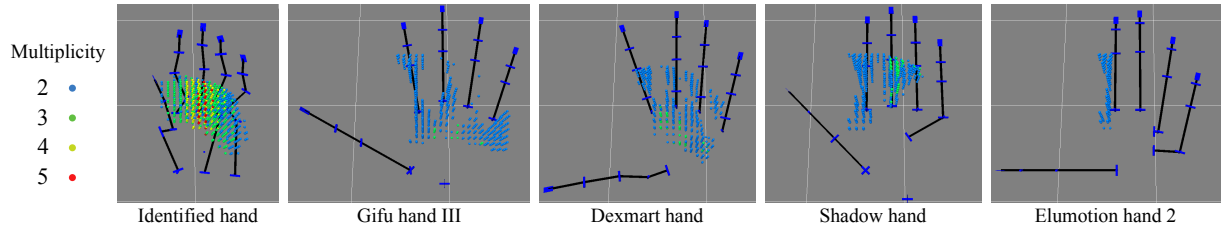

Fig. 10. Comparison of the distribution of pinchability (DOP) of some anthropomorphic robot hands

[12] T. Sugihara, "Solvability-Unconcerned Inverse Kinematics by the Levenberg-Marquardt Method," *IEEE Transaction on Robotics*, vol. 27, no. 5, pp. 984–991, 2011.

[13] S. Hayti and M. Mirmirani, "Improving the Absolute Positioning Accuracy of Robot Manipulators," *Journal of Robotic Systems*, vol. 2, no. 4, pp. 397–413, 1985.

[14] J. A. Nelder and R. Mead, "A simplex method for function minimization," *Computer Journal*, vol. 7, pp. 308–313, 1965.

[15] T. Mouri, H. Kawasaki, K. Yoshikawa, J. Takai, and S. Ito, "Anthropomorphic robot hand "gifu hand III"," in *International Congress and Convention Association*, 2002, pp. 1288–1293.

[16] https://www.shadowrobot.com/.

[17] G. Palli, C. Melchiorri, G. Vassura, U. Scarcia, L. Moriello, G. Berselli, A. Cavallo, G. D. Maria, C. Natale, S. Pirozzi, C. May, F. Ficuciello, and B. Siciliano, "The dexmart hand: Mechatronic design and experimental evaluation of synergy-based control for human-like grasping," *International Journal of Robotics Research*, vol. 33, pp. 799–824, 2014.

[18] http://elumotion.com/index.php/portfolio/project-title-1.